

Spin glass behavior of semiconducting $K_xFe_{2-y}S_2$

Hechang Lei, Milinda Abeykoon, Emil S. Bozin, and C. Petrovic

Condensed Matter Physics and Materials Science Department,

Brookhaven National Laboratory, Upton, NY 11973, USA

(Dated: February 16, 2022)

We report discovery of $K_xFe_{2-y}S_2$ single crystals, isostructural to $K_xFe_{2-y}Se_2$ superconductors. The sulfide compound is a small gap semiconductor and shows spin glass behavior below 32 K. Our results indicate that stoichiometry, defects and local environment of FeCh (Ch = S, Se) tetrahedra have important effects on the physical properties of isostructural and isoelectronic $K_xFe_{2-y}Ch_2$ compounds.

PACS numbers: 74.70.Xa, 74.70.Ad, 75.50.Lk, 74.72.Cj

Iron based materials are in the focus of exploratory search for new superconductors since the discovery of $LaFeAsO_{1-x}F_x$ with transition temperature T_c up to 26 K.¹ Several superconducting families were discovered soon after $REFePnO$ (RE = rare earth; Pn = P or As, FePn-1111 type),²⁻⁴ including α -PbO type FeCh (Ch = S, Se, and Te, FeCh-11 type) materials that do not have any crystallographic layer in between puckered Fe-Ch slabs.⁴ FeCh-11 type materials share a square-planar lattice of Fe with tetrahedral coordination and similar Fermi surface topology with other iron-based superconductors.⁵ Under external pressure,^{6,7} the T_c can be increased from 8 K to 37 K and the dT_c/dP can reach 9.1 K/GPa, the highest in all iron-based superconductors.⁷ The empirical rule proposed by Mizuguchi et al. proposes that the critical temperature is closely correlated with the anion height between Fe and Ch layers. There is an optimal distance around 0.138 nm with a maximum transition temperature $T_c \simeq 55$ K.⁸

Intercalation can change the local environment of Fe-Se tetrahedron and introduce extra carriers. The intercalation could also decrease dimensionality of conducting bands. This is favorable for superconductivity since the presence of low energy electronic collective modes in layered conductors helps to screen Coulomb interaction.⁹ This is seen in iron based superconductors: the T_c increases from FeCh-11 type to FePn-1111 type. Very recently the superconducting T_c is enhanced in iron selenide material to about 30 K not by external pressure but by inserting K, Rb, Cs, and Tl between the FeSe layers (AFSe-122 type), thus changing the crystal structure around FeCh tetrahedra.¹⁰⁻¹³ Similar to pressure effects, the intercalation using elements with +1 valence decreases Se height towards the optimum value.¹² The expanded Fe-Se interlayer distances could also contribute to reducing dimensionality of conducting bands and magnetic interactions. On the other hand, the insulating-superconducting transition (IST) can be induced in $(Tl_{1-x}K_x)Fe_{2-y}Se_2$ by tuning the Fe stoichiometry and implying that the superconductivity is in proximity of an antiferromagnetic (AFM) Mott insulating state.¹³ Thus exploring new oxychalcogenide and chalcogenide compounds containing similar FeCh layers would be instructive.

In this work, we report discovery of $K_xFe_{2-y}S_2$ single crystals isostructural to 122 iron selenide superconductors. The structure analysis indicates that the anion height might not be essential for superconductivity. The resistivity and magnetic measurements suggest spin glass (SG) semiconductor ground state similar to the $TlFe_{2-x}Se_2$ with high Fe deficiency, even though anion height are close to values found in iron based superconductors with T_c above 20 K.^{13,14}

Single crystals of $K_xFe_{2-y}S_2$ were grown by self-flux method¹⁵ with nominal composition K:Fe:S = 0.8:2:2. Prereacted FeS and K pieces were added into the alumina crucible with partial pressure of argon gas. The quartz tubes were heated to 1030 °C, kept at this temperature for 3 hours, then cooled to 730 °C. Platelike crystals up to $10 \times 10 \times 3$ mm³ can be grown. Powder X-ray diffraction (XRD) data were collected at 300 K using 0.3184 Å wavelength radiation (38.94 keV) at X7B beamline of the National Synchrotron Light Source. The average stoichiometry was determined by energy-dispersive x-ray spectroscopy (EDX). Electrical transport, heat capacity, and magnetization measurements were carried out in Quantum Design PPMS-9 and MPMS-XL5.

Fig. 1(a) shows powder XRD data at the room temperature and structural refinements on $K_xFe_{2-y}S_2$ using General Structure Analysis System (GSAS).^{16,17} Model possessing tetragonal $ThCr_2Si_2$ structure, space group $I4/mmm$, failed to explain the observed diffraction pattern, due to clear appearance of (110) and other superlattice reflections indicating symmetry lowering to $I4/m$. Data were successfully explained within $I4/m$ symmetry that incorporates Fe vacancy order site, with lattice parameters $a = 8.3984(5)$ Å and $c = 13.5988(11)$ Å, appreciably smaller than those observed in the selenium counterpart.¹⁰ The c axis is particularly reduced due to the smaller ionic size of S^{2-} when compared to Se^{2-} . The ordered Fe vacancy is the same as in $K_xFe_{2-y}Se_2$.¹⁸ This may imply similar origin of magnetic behavior for both compounds. Atomic positions with refined parameters are listed in Table 1. Refinements yielded that K1, K2 and Fe1 positions are partially occupied, while Fe2 are almost fully occupied. It should be noted that when K1 and Fe1 positions are fully unoccupied while K2 and Fe2 are fully occupied, the corresponding chemical for-

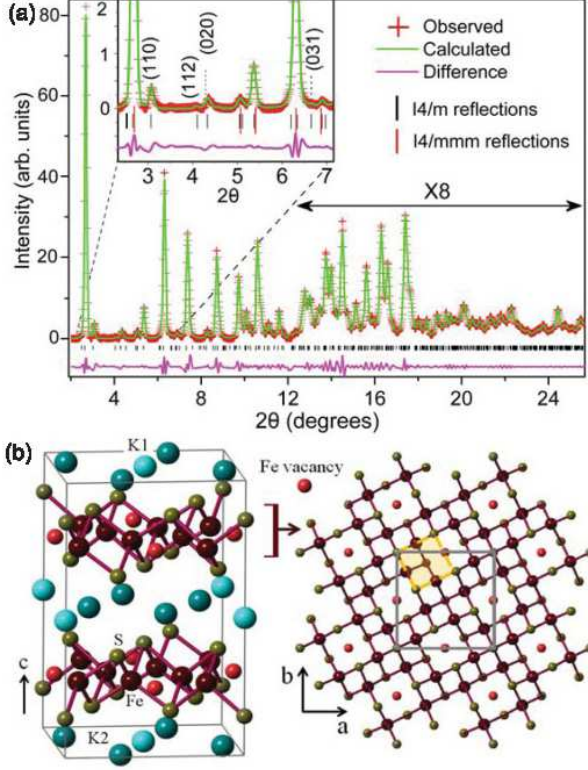


FIG. 1. (a) Powder XRD patterns of $K_xFe_{2-y}S_2$ and fit using I4/m model. Inset: low scattering angle part, emphasizing presence of superlattice reflections characteristic of I4/m symmetry. Enlarged isotropic thermal parameters, particularly in the potassium layer, are indicative of local disorder being present in the structure. (b) Crystal structure of $K_xFe_{2-y}S_2$ in I4/m unit cell with vacant Fe1 sites marked red and K1 sites marked light blue (left). Sketch of the FeS slab (c-axis view), with ordered Fe vacancies (right). Yellow and grey squares illustrate I4/mmm and I4/m unit cells respectively.

mula is $K_{0.8}Fe_{1.6}S_2$ and the Fe vacancy is completely ordered. The average atomic ratios from EDX are consistent with $K_{0.88(6)}Fe_{1.63(4)}S_{2.00(1)}$, indicating that there are both potassium and iron deficiencies from ideal 122 stoichiometry, in good agreement with XRD fitting results. It should be noted that the 18.5% of the iron precipitates on the surface of the ingot on cooling. The iron precipitates are easy to remove and have no influence on the physical properties of $K_xFe_{2-y}S_2$.

The in-plane resistivity $\rho_{ab}(T)$ of the $K_xFe_{2-y}S_2$ single crystal rapidly increases with decreasing the temperature from $\rho_{ab}(300\text{ K}) \sim 100\text{ m}\Omega\text{ cm}$ and there is no obvious magnetoresistance (Fig. 2). The $\rho_{ab}(T)$ is thermally activated: $\rho = \rho_0 \exp(E_a/k_B T)$, where ρ_0 is a prefactor and k_B is the Boltzmann's constant (inset (b) of Fig 2). Using the $\rho_{ab}(T)$ data from 70 to 300 K, we estimate $\rho_0 \sim 11.7(2)\text{ m}\Omega\text{ cm}$ and the activation energy $E_a = 51.8(2)\text{ meV}$. The semiconducting behavior might

TABLE I. Structural parameters for $K_xFe_{2-y}S_2$ at room temperature. Values in brackets give the number of equivalent distances or angles of each type.

Chemical Formula			K _{0.88} Fe _{1.63} S ₂		
Space Group			I4/m		
a (Å)			8.3984(5)		
c (Å)			13.5988(11)		
V (Å ³)			959.17(11)		
Interatomic Distances (Å)			Bond Angles (°)		
d _{Fe1-S2} [4]	2.4170(12)	S2-Fe1-S2 [2]	110.1(5)		
d _{Fe1-Fe2} [4]	2.5914(16)	S2-Fe1-S2 [4]	109.2(3)		
d _{Fe2-S1} [1]	2.3647(11)	S1-Fe2-S2 [1]	103.9(5)		
d _{Fe2-S2} [1]	2.3369(11)	S1-Fe2-S2 [1]	109.8(3)		
d _{Fe2-S2} [1]	2.3005(11)	S1-Fe2-S2 [1]	111.0(3)		
d _{Fe2-S2} [1]	2.2660(11)	S2-Fe2-S2 [1]	105.3(3)		
d _{Fe2-Fe2} [2]	2.6495(16)	S2-Fe2-S2 [1]	117.7(2)		
d _{Fe2-Fe2} [1]	2.8135(17)	S2-Fe2-S2 [1]	108.7(5)		
Anion Heights (Å)					
S1 to Fe1	1.388(5)	S2 to Fe1	1.384(5)		
S1 to Fe2	1.334(5)	S2 to Fe2	1.439(5)		
Atom	x	y	z	Occ	U _{iso} (Å ²)
K1	0	0	0.5	0.84(12)	0.059(15)
K2	0.80(2)	0.418(6)	0.5000	0.89(3)	0.059(15)
Fe1	0	0.5	0.25	0.08(4)	0.0136(3)
Fe2	0.2954(5)	0.4111(5)	0.2460(16)	1.00(1)	0.0136(3)
S1	0	0	0.1479(5)	1.00(0)	0.0111(6)
S2	0.1113(4)	0.292(1)	0.3518(3)	1.00(0)	0.0111(6)

at least partially be ascribed to the deficiency of Fe in Fe-Se plane that would introduce random scattering potential, just like in highly Fe deficient $K_xFe_{2-y}Se_2$ and $TlFe_{2-x}Se_2$.^{13,14,19}

The magnetic susceptibility with $H \parallel ab$ is larger than with $H \parallel c$ (Fig. 3(a)), similar to observed anisotropy in $TlFe_{2-x}Se_2$.¹⁴ The most interesting characteristics are the absence of Curie-Weiss behavior and obvious bifurcation between the zero-field-cooling (ZFC) and field-cooling (FC) curves below 32 K. This might suggest the presence of low-dimensional short range magnetic correlations and/or a long range magnetic order above 300 K, and an antiferromagnetic phase transition at low temperatures. The $M(T)$ irreversible behavior below 32 K implies some ferromagnetic contribution to magnetic susceptibility or a glassy transition where spins would be frozen randomly below the freezing temperature T_f . Similar magnetization has been reported in $TlFe_{2-x}Se_2$ and $KFeCuS_2$.^{14,20} Inset in Fig. 3 (a) shows the magnetization loops for $H \parallel c$. At 250 K, the M-H loop is almost linear and there is no hysteresis. However, an s-shape M-H loop can be observed at 1.8 K, which is a typical behavior of a SG system.¹⁴ The s-shape M-H loop is present at $T = 50\text{ K}$ which indicates that short-range ferromagnetic interaction may exist above T_f . As shown

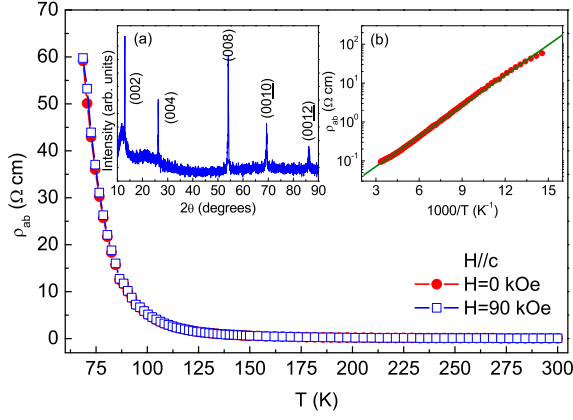


FIG. 2. Temperature dependence of the in-plane resistivity $\rho_{ab}(T)$ with $H = 0$ (closed red circles) and 90 kOe (open blue squares). Inset (a) shows the single crystal XRD pattern of $K_xFe_{2-y}S_2$ obtained using Rigaku Miniflex. The crystal surface is normal to the c axis with the plate-shaped surface parallel to the ab -plane. Inset (b) shows the fitting result using thermally activated model for $\rho_{ab}(T)$ in zero field.

in Fig. 3(b), the peak in the real part of ac susceptibility $\chi'(T)$ exhibits strong frequency dependence in ac magnetic field. When the frequency increases, the peak positions shift to higher temperatures whereas the magnitudes decrease, indicating a typical SG behavior.²¹ By fitting the frequency dependence of the peak shift using $K = \Delta T_f / (T_f \Delta \log f)$, we obtained $K = 0.0134(5)$. This is in agreement with values ($0.0045 \leq K \leq 0.08$) found in the canonical SG system, but much smaller than in typical superparamagnet.²¹ Fig. 3(c) shows the magnetic field dependence of the thermoremanent magnetization (TRM). The sample was cooled from $T = 60$ K (above T_f) in a magnetic field to $T = 10$ K (below T_f) and then kept at 10 K for a $t_w = 100$ s. Then, the magnetic field was removed and the magnetization decay $M_{TRM}(t)$ was measured. It can be seen that, below T_f ($T = 10$ K), $M_{TRM}(t)$ decays slowly so that its value is non-zero even after several hours. This is another signature of the SG behavior, i.e., the existence of extremely slow spin relaxation below T_f .²¹ In contrast, above T_f , $M_{TRM}(t)$ quickly relaxes and does not show slow decay (inset (a) of Fig. 3(c)). The magnetization decay can be explained well using a stretched exponential function commonly used to explain TRM behavior in SG systems, $M_{TRM}(t) = M_0 \exp[-(t/\tau)^{1-n}]$, where M_0 , τ , and $1-n$ are the glassy component, the relaxation characteristic time, and the critical exponent, respectively. It can be seen (inset (b) of Fig. 3(c)) that τ decreases significantly with field but the $1-n$ increases slightly. On the other hand, the value of $1-n$ is close to $1/3$, consistent with theoretical predictions and the experiments on traditional SG system.^{22,23} The SG behavior could originate from Fe clusters induced by vacancies and disorder, and the exchange interactions between spins within a cluster would depend on the distribution of iron ions (Table 1).²⁰ Indeed, in $TlFe_{2-x}Se_2$, the ground state is a reentrant

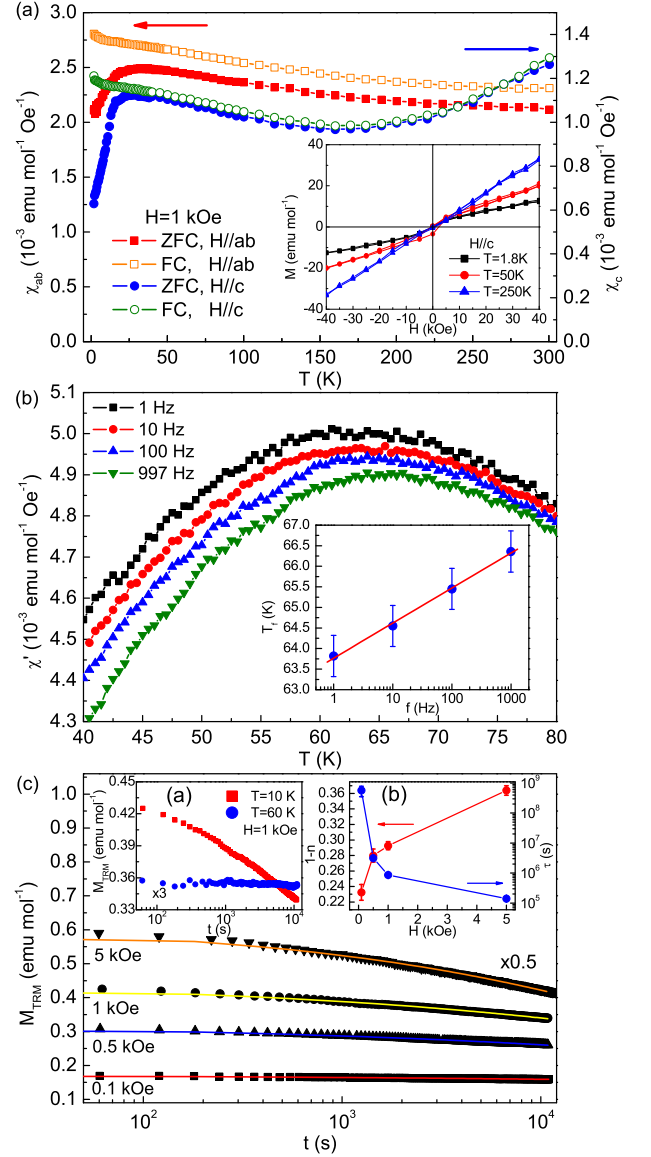


FIG. 3. (a) ZFC and FC dc magnetic susceptibility with $H \parallel c$ and $H \parallel ab$ below 300 K. Inset: isothermal $M(H)$ for $H \parallel c$ at $T = 1.8, 50$, and 250 K. (b) Temperature dependence of $\chi'(T)$ measured at several fixed frequencies. Inset: the frequency dependence of T_f . The solid line is the linear fit to the T_f data. (c) M_{TRM} vs. t at 10 K with various dc fields and $t_w = 100$ s. The solid lines are fits using a stretched exponential function. Inset (a): M_{TRM} vs. t at 10 K and 60 K with $H = 1$ kOe and $t_w = 100$ s. Inset (b): magnetic field dependence of $1-n$ and τ .

spin glass if the content of Fe is below 1.7.¹⁴ However, for x values larger than 1.7, $TlFe_{2-x}Se_2$ becomes a superconductor below 20 K.¹³ Therefore superconductivity in $K_xFe_{2-y}S_2$ might be induced for smaller deficiency of Fe.

Specific heat of $K_xFe_{2-y}S_2$ (Fig. 4) approaches the Dulong-Petit value of $3NR$ at high temperature, where N is the atomic number in the chemical formula ($N = 5$) and R is the gas constant. At low temperature, specific heat

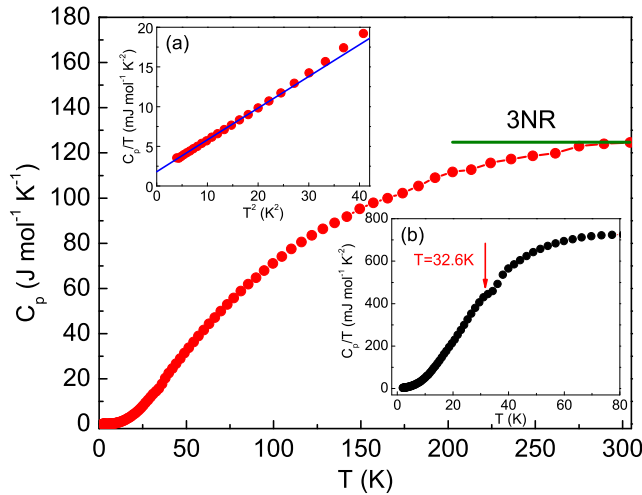


FIG. 4. Temperature dependence of specific heat. Inset (a) shows the low-temperature specific-heat data in the plot of C_p/T vs T^2 . The blue solid line is the fitting curves using formula $C_p/T = \gamma_{SG} + \beta T^2$. Inset (b) shows the enlarged area near magnetic transition region of C_p/T - T .

can be fitted using $C_p = \gamma_{SG}T + \beta T^3$ (inset (a) of Fig. 4). The γ_{SG} is commonly found in magnetic insulating SG system, implying constant density of states of the low temperature magnetic excitations.^{24–26} The second term is due to phonon contribution. The obtained γ_{SG} is 1.58(6) mJ/mol-K². The Debye temperatures Θ_D can be calculated from β through $\Theta_D = (12\pi^4 NR/5\beta)^{1/3}$ to be $\Theta_D = 284.3(7)$ K. It should be noted that, as opposed to usual λ anomaly, there is a very weak broad hump of C_p/T near $T = 32.6$ K (inset (b) of Fig. 4). This

is expected for bulk low dimensional or glassy magnetic systems.^{24,27,28}

Discovery of $K_x\text{Fe}_{2-y}\text{S}_2$ implies that it is possible to tune conductivity and magnetism by changing chalcogen elements (S and Se) in isostructural $K_x\text{Fe}_{2-y}\text{Ch}_2$ materials. According to the Table 1, anion heights S1 to Fe1 and S1 to Fe2 in $K_{0.88(6)}\text{Fe}_{1.63(4)}\text{S}_{2.00(1)}$ are close to the alleged optimal value of 1.38 Å, comparable to distances in FePn-1111 type materials and lower than in $K_x\text{Fe}_{2-y}\text{Se}_2$.^{8,12} Hence, if the anion height is the crucial parameter, the sulfide compound should be a superconductor with higher T_c than $K_x\text{Fe}_{2-y}\text{Se}_2$. However, it is a semiconductor not a superconductor. We also note that in $K_x\text{Fe}_{2-y}\text{S}_2$ there are two Fe sites and two corresponding anion heights. Our results indicate that the anion height values may be not essential parameters that govern superconductivity in AFeSe-122 compounds. In contrast, it suggests that disorder and site occupancies are significantly important.

In summary, we report discovery of $K_x\text{Fe}_{2-y}\text{S}_2$ single crystals isostructural to $T_c = 33$ K superconductor $K_x\text{Fe}_{2-y}\text{Se}_2$ and exhibiting similar width of formation and vacancies on both potassium and iron site. Sulfide material is semiconducting and glassy magnetic suggesting that the physical properties are governed by stoichiometry, defects, local environment of Fe-S tetrahedra.

We thank S. L. Bud'ko for discussions, John Warren for help with SEM measurements and John Hanson for help in facilitating X7B experiment. Work at Brookhaven is supported by the U.S. DOE under Contract No. DE-AC02-98CH10886 and in part by the Center for Emergent Superconductivity, an Energy Frontier Research Center funded by the U.S. DOE, Office for Basic Energy Science.

- ¹ Y. Kamihara, T. Watanabe, M. Hirano, and H. Hosono, *J. Am. Chem. Soc.* **130**, 3296 (2008).
- ² M. Rotter, M. Tegel, and D. Johrendt, *Phys. Rev. Lett.* **101**, 107006 (2008).
- ³ X. C. Wang, Q. Q. Liu, Y. X. Lv, W. B. Gao, L. X. Yang, R. C. Yu, F. Y. Li, and C. Q. Jin, *Solid State Commun.* **148**, 538 (2008).
- ⁴ F. C. Hsu, J. Y. Luo, K. W. Yeh, T. K. Chen, T. W. Huang, P. M. Wu, Y. C. Lee, Y. L. Huang, Y. Y. Chu, D. C. Yan, and M. K. Wu, *Proc. Natl. Acad. Sci. USA* **105**, 14262 (2008).
- ⁵ A. Subedi, L. Zhang, D. J. Singh, and M. H. Du, *Phys. Rev. B* **78**, 134514 (2008).
- ⁶ Y. Mizuguchi, F. Tomioka, S. Tsuda, T. Yamaguchi, and Y. Takano, *Appl. Phys. Lett.* **93**, 152505 (2008).
- ⁷ S. Medvedev, T. M. McQueen, I. Trojan, T. Palasyuk, M. I. Erements, R. J. Cava, S. Naghavi, F. Casper, V. Ksenofontov, G. Wortmann, and C. Felser, *Nature Mater.* **8**, 630 (2009).
- ⁸ Y. Mizuguchi, Y. Hara, K. Deguchi, S. Tsuda, T. Yamaguchi, K. Takeda, H. Kotegawa, H. Tou, and Y. Takano, *Supercond. Sci. Technol.* **23**, 054013 (2010).
- ⁹ A. Bill, H. Morawitz, and V. Z. Kresin, *Phys. Rev. B* **68**,

- 144519 (2003)
- ¹⁰ J. Guo, S. Jin, G. Wang, S. Wang, K. Zhu, T. Zhou, M. He, and X. Chen, *Phys. Rev. B* **82**, 180520(R) (2010).
- ¹¹ A. F. Wang, J. J. Ying, Y. J. Yan, R. H. Liu, X. G. Luo, Z. Y. Li, X. F. Wang, M. Zhang, G. J. Ye, P. Cheng, Z. J. Xiang, and X. H. Chen, *Phys. Rev. B* **83**, 060512(R) (2011).
- ¹² A. Krzton-Maziopa, Z. Shermadini, E. Pomjakushina, V. Pomjakushin, M. Bendele, A. Amato, R. Khasanov, H. Luetkens, and K. Conder, *J. Phys.: Condens. Matter* **23**, 052203 (2011).
- ¹³ M. H. Fang, H. D. Wang, C. H. Dong, Z. J. Li, C. M. Feng, J. Chen, and H. Q. Yuan, *Europhys. Lett.* **94**, 27009 (2011).
- ¹⁴ J. J. Ying, A. F. Wang, Z. J. Xiang, X. G. Luo, R. H. Liu, X. F. Wang, Y. J. Yan, M. Zhang, G. J. Ye, P. Cheng, and X. H. Chen, *arXiv:1012.2929*.
- ¹⁵ K. Kihou, T. Saito, S. Ishida, M. Nakajima, Y. Tomioka, H. Fukazawa, Y. Kohori, T. Ito, S. Uchida, A. Iyo, C. Lee, and H. Eisaki, *J. Phys. Soc. Jpn.* **79**, 124713 (2010).
- ¹⁶ A. C. Larson and R. B. Von Dreele, Los Alamos National Laboratory Report LAUR 86-748 (1994).
- ¹⁷ B. H. Toby, *J. Appl. Cryst.* **34**, 210 (2001).

- ¹⁸ W. Bao, Q. Huang, G. F. Chen, M. A. Green, D. M. Wang, J. B. He, X. Q. Wang, and Y. Qiu, arXiv:1102.0830 (2011).
- ¹⁹ D. M. Wang, J. B. He, T.-L. Xia, and G. F. Chen, Phys. Rev. B **83**, 132502 (2011).
- ²⁰ M. Oledzka, K. V. Ramanujachary, and M. Greenblatt, Mater. Res. Bull. **31**, 1491 (1996).
- ²¹ J. A. Mydosh, Spin Glasses: An Experimental Introduction Taylor & Francis, London, 1993.
- ²² I. A. Campbell, Phys. Rev. B **37**, 9800 (1988).
- ²³ D. Chu, G. G. Kenning, and R. Orbach, Phys. Rev. Lett. **72**, 3270 (1994).
- ²⁴ C. Y. Huang, J. Magn. Magn. Mater. **51**, 1 (1985).
- ²⁵ D. Meschede, F. Steglich, W. Felsch, H. Maletta, and W. Zinn, Phys. Rev. Lett. **44**, 102 (1980).
- ²⁶ N. P. Raju, E. Gmelin, and R. K. Kremer, Phys. Rev. B **46**, 5405 (1992).
- ²⁷ G. E. Brodale, R. A. Fisher, W. E. Fogle, N. E. Phillips, and J. van Curen, J. Magn. Magn. Mater. **31-34**, 1331 (1983).
- ²⁸ L. O.-S. Martin, J. P. Chapman, L. Lezama, J. J. S. Garitaonandia, J. S. Marcos, J. Rodríguez-Fernández, M. I. Arriortua, and T. Rojo, J. Mater. Chem. **16**, 66 (2006).